



**HAL**  
open science

## **Influence of the microenvironment on modulation of the host response by typhoid toxin**

Océane Martin, Anna Bergonzini, Maria Lopez Chiloeches, Eleni Paparouna, Deborah Butter, Sofia D P Theodorou, Maria M Haykal, Elisa Boutet-Robinet, Toma Tebaldi, Andrew Wakeham, et al.

### ► To cite this version:

Océane Martin, Anna Bergonzini, Maria Lopez Chiloeches, Eleni Paparouna, Deborah Butter, et al.. Influence of the microenvironment on modulation of the host response by typhoid toxin. Cell Reports, 2021, 35 (1), pp.108931. 10.1016/j.celrep.2021.108931 . hal-03201865

**HAL Id: hal-03201865**

**<https://hal.inrae.fr/hal-03201865>**

Submitted on 19 Apr 2021

**HAL** is a multi-disciplinary open access archive for the deposit and dissemination of scientific research documents, whether they are published or not. The documents may come from teaching and research institutions in France or abroad, or from public or private research centers.

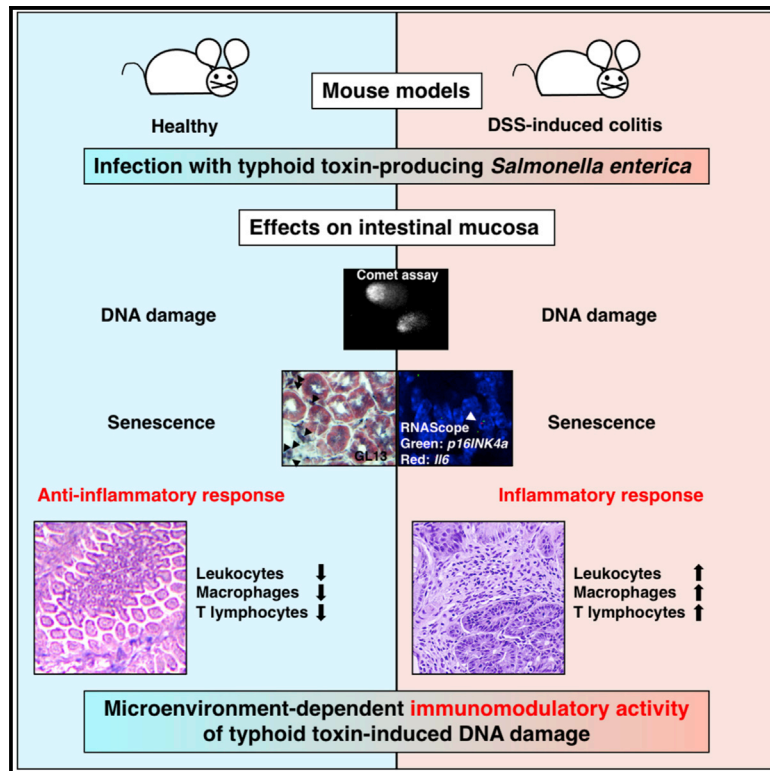
L'archive ouverte pluridisciplinaire **HAL**, est destinée au dépôt et à la diffusion de documents scientifiques de niveau recherche, publiés ou non, émanant des établissements d'enseignement et de recherche français ou étrangers, des laboratoires publics ou privés.



Distributed under a Creative Commons Attribution 4.0 International License

## Influence of the microenvironment on modulation of the host response by typhoid toxin

### Graphical abstract



### Authors

Océane C.B. Martin, Anna Bergonzini, Maria Lopez Chiloeches, ..., Tak Mak, Ioannis S. Pateras, Teresa Frisan

### Correspondence

teresa.frisan@umu.se

### In brief

Using as model a typhoid-toxin-producing *Salmonella* Typhimurium, Martin et al. highlight a complex microenvironment-dependent crosstalk between the bacterial-genotoxin-induced DNA damage response and regulation of the host immune response, underlining the role of bacterial genotoxins as immunomodulators.

### Highlights

- Typhoid toxin causes DNA fragmentation *in vivo* not associated with inflammation
- Infection with a genotoxin-producing bacterium induces senescence *in vivo*
- The presence of senescent cells is associated with an anti-inflammatory response
- The anti-inflammatory effect is lost in mice with acute colitis



## Article

# Influence of the microenvironment on modulation of the host response by typhoid toxin

Océane C.B. Martin,<sup>1,14</sup> Anna Bergonzini,<sup>2,3</sup> Maria Lopez Chiloeches,<sup>2,3</sup> Eleni Paparouna,<sup>4</sup> Deborah Butter,<sup>1,15</sup> Sofia D.P. Theodorou,<sup>4</sup> Maria M. Haykal,<sup>5</sup> Elisa Boutet-Robinet,<sup>6</sup> Toma Tebaldi,<sup>7</sup> Andrew Wakeham,<sup>8</sup> Mikael Rhen,<sup>9</sup> Vassilis G. Gorgoulis,<sup>4,10,11,12</sup> Tak Mak,<sup>8</sup> Ioannis S. Pateras,<sup>4,13</sup> and Teresa Frisan<sup>1,2,3,13,16,\*</sup>

<sup>1</sup>Department of Cell and Molecular Biology, Karolinska Institutet, Stockholm, Sweden

<sup>2</sup>Department of Molecular Biology, Umeå University, Umeå, Sweden

<sup>3</sup>Umeå Centre for Microbial Research (UCMR), Umeå University, Umeå, Sweden

<sup>4</sup>Department of Histology and Embryology, School of Medicine, National and Kapodistrian University of Athens, Athens, Greece

<sup>5</sup>Université Paris-Saclay, Institut Gustave Roussy, Inserm U981, Biomarqueurs prédictifs et nouvelles stratégies thérapeutiques en oncologie, 94800 Villejuif, France

<sup>6</sup>Toxalim (Research Centre in Food Toxicology), Université de Toulouse, INRAE, ENVT, INP-Purpan, UPS, Toulouse, France

<sup>7</sup>Center for Biomedical Data Science, Yale School of Medicine, New Haven, CT, USA

<sup>8</sup>The Campbell Family Institute for Breast Cancer Research, Princess Margaret Hospital, University of Toronto, Toronto, ON, Canada

<sup>9</sup>Department of Microbiology, Tumor and Cell Biology, Karolinska Institutet, Stockholm, Sweden

<sup>10</sup>Biomedical Research Foundation, Academy of Athens, Athens, Greece

<sup>11</sup>Institute for Cancer Sciences, University of Manchester, Manchester Academic Health Science Centre, Manchester, UK

<sup>12</sup>Manchester Centre for Cellular Metabolism, University of Manchester, Manchester Academic Health Science Centre, Manchester, UK

<sup>13</sup>These authors contributed equally

<sup>14</sup>Present address: University of Bordeaux, INSERM, UMR1053 Bordeaux Research in Translational Oncology, BaRITOn, Bordeaux, France

<sup>15</sup>Present address: Department of Cancer Biology, Dana-Farber Cancer Institute, Boston, MA 02215, USA

<sup>16</sup>Lead contact

\*Correspondence: [teresa.frisan@umu.se](mailto:teresa.frisan@umu.se)

<https://doi.org/10.1016/j.celrep.2021.108931>

## SUMMARY

**Bacterial genotoxins cause DNA damage in eukaryotic cells, resulting in activation of the DNA damage response (DDR) *in vitro*. These toxins are produced by Gram-negative bacteria, enriched in the microbiota of inflammatory bowel disease (IBD) and colorectal cancer (CRC) patients. However, their role in infection remains poorly characterized. We address the role of typhoid toxin in modulation of the host-microbial interaction in health and disease. Infection with a genotoxigenic *Salmonella* protects mice from intestinal inflammation. We show that the presence of an active genotoxin promotes DNA fragmentation and senescence *in vivo*, which is uncoupled from an inflammatory response and unexpectedly associated with induction of an anti-inflammatory environment. The anti-inflammatory response is lost when infection occurs in mice with acute colitis. These data highlight a complex context-dependent crosstalk between bacterial-genotoxin-induced DDR and the host immune response, underlining an unexpected role for bacterial genotoxins.**

## INTRODUCTION

Typhoid toxin (TT) and cytolethal distending toxins (CDTs), produced by several Gram-negative bacteria, belong to a family of bacterial protein effectors that cause DNA damage in eukaryotic cells (Grasso and Frisan, 2015). CDTs and TT are tripartite toxins that share the CdtB active subunit, a structural and functional homolog of mammalian DNase I (Nesić et al., 2004; Song et al., 2013). Upon delivery into the nucleus of the target cells, the CdtB subunit induces DNA strand breaks, which activate the DNA damage response (DDR), coordinated by the sensor kinase ataxia telangiectasia mutated (ATM) (Grasso and Frisan, 2015). As a consequence of DDR activation, the intoxicated cells are arrested in the G1 and/or G2 phases of the cell cycle and initiate

DNA repair. However, if the extent of the damage is beyond repair, most cell types undergo senescence (Blazkova et al., 2010; Ibler et al., 2019; Secher et al., 2013). Occasionally, intoxicated cells may survive and overcome the DDR-induced tumorigenic barrier, leading to genomic instability and acquisition of carcinogenic traits (Guidi et al., 2013a; Hanahan and Weinberg, 2011).

DNA-damage-induced cellular senescence is characterized by (1) a generally permanent cell-cycle arrest, induced by activation of the cyclin-dependent kinase inhibitors p16<sup>INK4a</sup>, p15<sup>INK4b</sup>, and p21<sup>CIP1/WAF1</sup>; and (2) an active metabolic state resulting in secretion of a broad panel of mediators, most of them with a pro-inflammatory profile, including cytokines (interleukin-1 $\alpha$  [IL-1 $\alpha$ ], IL-6, and IL-8), growth factors (Hepatocyte growth factor [HGF] and Granulocyte macrophage colony-stimulating factor



[GM-CSF]), and matrix metalloproteases (MMP1-1 and MMP-3) (Gorgoulis et al., 2019). The latter has also been defined as a senescence-associated secretory phenotype (SASP) (Campisi and d'Adda di Fagagna, 2007; Krtolica et al., 2001). The pro-inflammatory response induced by DNA damage can be further fueled by type I interferon (IFN) secretion induced by the recognition of cytosolic DNA fragments through the cGAS (cyclic GMP-AMP synthase)-STING (Stimulator of Interferon Genes) pathway (Härtlova et al., 2015; Li and Chen, 2018).

Considering the mode of action and the plethora of non-cell-autonomous effects that senescent cells exert in the surrounding microenvironment, it is puzzling that certain bacteria have acquired genotoxins, since it is unlikely that their primary purpose is to induce or promote cancer in the mammalian host. To understand the role of these bacterial effectors during infection, we have assessed the role of a functional TT, which is produced by *Salmonella* Typhi (Haghjoo and Galán, 2004). However, studying the effect of the TT *in vivo* poses a challenge, since this bacterium is a strict human pathogen. Therefore, we used as model *Salmonella enterica*, serovar Typhimurium (*S. Typhimurium*), which causes a systemic typhoid-like infection in immunocompetent mice upon oral infection (Carter and Collins, 1974; Clements et al., 2002; Haghjoo and Galán, 2004; Spanò et al., 2008). Since *S. Typhimurium* does not harbor the toxin genes, we developed a set of strains expressing either an active or inactive TT (Del Bel Belluz et al., 2016). We have previously shown that expression of a functional toxin in the non-typhoidal *S. Typhimurium* represses the intestinal mucosal inflammatory response normally elicited by this serovar (Del Bel Belluz et al., 2016), suggesting that this effector can exert an immunomodulatory activity, thus contributing to the stealth invasion characteristic of *S. Typhi* (Dougan and Baker, 2014). To test this hypothesis, we thoroughly compared the immune response induced by TT-expressing *S. Typhimurium* (herein defined as genotoxigenic) in an *in vivo* model of acute infection.

We demonstrate that infection with a strain expressing a functional TT, even though inducing DNA fragmentation, protects mice from intestinal inflammation. The response was characterized by induction of senescence, nuclear factor  $\kappa$ B (NF- $\kappa$ B) activation, reduced recruitment of leukocytes and T lymphocytes, production of T helper 2 (Th2) cytokines, and a higher percentage of anti-inflammatory macrophages and regulatory T cells. This anti-inflammatory effect, partially dependent on a functional ATM, was lost when infection with the genotoxigenic strain occurred in subjects with preexisting acute colitis, highlighting the influence of the tissue microenvironment on the toxin immunomodulatory properties.

These data highlight three features that are relevant for the fields of infection biology and senescence: (1) infection with a genotoxin-producing bacterium causes DNA fragmentation *in vivo* that is not associated with a pro-inflammatory response, suggesting that the link between DNA damage and immune response is more complex than activation of the inflammatory response as consequence of danger sensing; (2) infection with a genotoxin-producing bacterium induces senescence *in vivo*; and (3) the presence of senescent cells is associated with an anti-inflammatory response. The results can have a broader

implication, since other bacterial genotoxins may also modulate the microenvironment and the outcome can be different, depending on the bacterium lifestyle and tissue tropism.

## RESULTS

### Infection with genotoxin-producing bacteria induces senescence *in vivo*

We have previously demonstrated that infection with *S. Typhimurium* expressing a functional TT enhances host survival and reduces the extent of the colonic inflammation in healthy mice (Del Bel Belluz et al., 2016). Here, we have extended this analysis by performing a more detailed characterization of the host response in Sv129 mice infected with the genotoxigenic *Salmonella* strain (here defined as MC1 TT) for 5 and 10 days. As a control, we used an isogenic strain lacking the genotoxigenic CdtB subunit (here defined as MC1  $\Delta$ cdtB). The presence of a functional TT enhanced the survival rate of infected mice compared to mice infected with the control strain (Figure S1A). Consistent with these data, histological evaluation performed at 10 days post-infection (dpi) revealed that mice infected with the MC1  $\Delta$ cdtB strain exhibited increased severity of enteritis and colitis compared to MC1-TT-treated mice, characterized by areas of superficial erosion and elevated neutrophilic infiltration in the lamina propria, along with increased number of Peyer's patches (PPs) (Figures 1A–1C, S2A, and S2B). This effect was not dependent on a different efficiency of colonization of the MC1 TT compared to the control strain (Figure S1B). The reduced inflammatory response was also detected in the small intestine of C57BL/6 mice infected with the attenuated genotoxigenic *Salmonella* strain MC71 (MC71 TT) carrying a mutation of polynucleotide phosphorylase (PNPase) gene (Clements et al., 2002) (Figure S3). Since we did not observe colonic inflammation in this mouse strain (data not shown), the analysis of the C57BL/6 model was focused on the small intestine.

These data indicate that the TT effect is very robust and can be observed independently of the mouse and *Salmonella* strains.

DNA damage induced by bacterial genotoxins *in vivo* has been commonly evaluated using surrogate markers of the DDR, such as the phosphorylated form of the histone H2AX at serine 139 ( $\gamma$ H2AX) (Rogakou et al., 1999). We assessed direct induction of DNA fragmentation in cells isolated from the intestinal mucosa using an alkaline comet-based assay, which is considered a gold-standard method to detect DNA strand breaks (Pu et al., 2015). Our data showed that a functional TT promotes DNA fragmentation to a greater extent than that observed in mice infected with control *Salmonella* (Figures 2A and S4). In spite of this observation, we detected enhanced levels of  $\gamma$ H2AX phosphorylation in the mucosa of mice infected with the MC1  $\Delta$ cdtB strain (Figures 2B and S5A), possibly due to the strong inflammatory response and consequent oxidative-stress-induced DNA double-strand breaks (DSBs) (Kay et al., 2019).

One of the consequences of DNA damage in cells exposed *in vitro* to bacterial genotoxins is the acquisition of senescence (Blazkova et al., 2010; Ibler et al., 2019), which is associated with secretion of a broad panel of mediators, mainly related to a pro-inflammatory effect, such as IL-1, IL-6, and IL-8 (Hernandez-Segura et al., 2018). Induction of the senescent

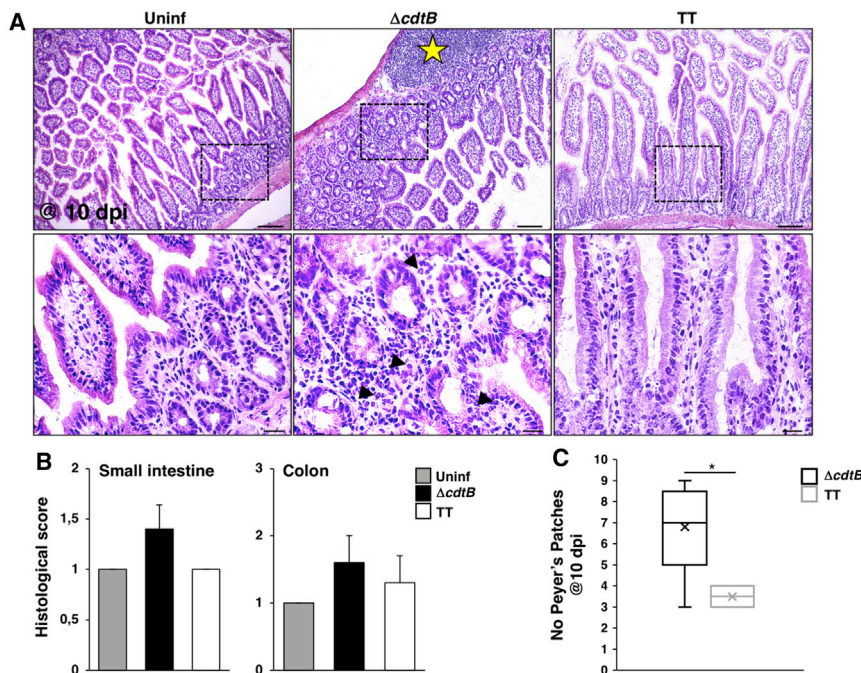


**Figure 1. Infection with the typhoid toxin (TT)-producing *Salmonella* reduces the inflammatory response**

Sv129 mice were mock infected with PBS (Uninf) or infected with the MC1  $\Delta cd t B$  ( $\Delta cd t B$ ) or MC1 TT (TT) strains for 10 days.

(A) Representative micrograph of the hematoxylin and eosin staining of the small intestine (necropsy performed at 10 dpi). The yellow asterisk indicates a Peyer's patch (PP), and the black arrowheads indicate infiltrating neutrophils in the lamina propria (scale bar, 100  $\mu$ m). The dotted squares in the upper panel indicate the regions shown at higher magnification in the lower panel (scale bar, 20  $\mu$ m). (B) Histological scores of small intestine and colon (n = 5 mice, mean  $\pm$  SEM). (C) Quantification of the macroscopically visible PPs. \*p  $\leq$  0.05 (n = 5 mice). See also Figures S1–S3.

Consistent with the time frame for activation of the adaptive immune response, infection with the MC1  $\Delta cd t B$  strain promoted increased levels of CD3 positive T lymphocytes at 10 dpi, while this effect was reduced in mice infected

with the genotoxigenic strain (Figure 3). To assess whether the DNA-damaging capacity of the TT promoted senescence in both Sv129 and C57BL/6 mice at the experimental endpoint of 10 dpi, we performed hybrid histo-/immunochemical staining employing the compound GL13 (also termed SenTraGor) that detects lipofuscin, a nondegradable aggregate of oxidized molecules that accumulates in the cytoplasm of senescent cells (Evangelou et al., 2017). As shown in Figures 2C and S5A, we detected a significant increase in GL13-positive epithelial cells in the colon and small intestine of mice infected with the MC1 TT and MC71 TT strains compared to levels detected in mice infected with control *Salmonella*. Higher levels of senescent cells in mice infected with the genotoxigenic strain were further confirmed by the increased percentage of cells co-expressing *p16INK4a* and *Ilf6* RNAs, two of the senescence hallmarks (Gorgoulis et al., 2019), assessed by RNAscope analysis, with a concordant result in both mouse strains analyzed (Figures 2D). This difference was not dependent on levels of *Ilf6* mRNA expression, which were similar in the infected mice, independently of bacterial strain (Figure S5C). Interestingly, we also detected a subpopulation of cells co-expressing mRNA-specific *p16INK4a* and *Ilf10*, which was significantly higher in Sv129 mice infected with the genotoxigenic strain and showed a similar trend in C57BL/6 mice (Figures S5D).

In summary, in our model, induction of senescence was uncoupled from the activation of a pro-inflammatory response (Figures 1, S2, and S3).

### TT maintains an anti-inflammatory microenvironment

Phenotypic analysis of the colonic immune cells showed a significant decrease in leukocytes (CD45) and macrophages (F4/80) at 5 dpi in mice infected with the MC1 TT strain compared to mice infected with control *Salmonella* (Figure 3).

with the genotoxigenic strain (Figure 3).

To further investigate whether the genotoxigenic *Salmonella* strain suppressed the activation of the host response or promoted a qualitatively different immune response with an anti-inflammatory profile, we investigated (1) activation of the transcription factor NF- $\kappa$ B by assessing nuclear translocation of the p65 subunit (Hayden et al., 2006), (2) the presence of non-inflammatory macrophages by detecting mannose receptor (CD206) (Shrivastava and Shukla, 2019), and (3) levels of mRNA expression of several pro- and anti-inflammatory effector molecules by qPCR and RNAscope analysis in the intestine of uninfected controls or mice infected with MC1 TT or MC1  $\Delta cd t B$  strains for 5 and 10 days.

*Salmonella* infection promoted an increase in the percentage of colonic stromal cells with a nuclear pattern of p65 staining compared to the levels observed in uninfected mice, and p65 nuclear translocation was most prominent at 10 dpi, independent of expression of an active genotoxin (Figure 4A; data not shown). However, in spite of a similar activation of NF- $\kappa$ B, infection with the genotoxigenic *Salmonella* was associated with a general reduction in mRNA levels of pro-inflammatory molecules associated with a Th1 response (most prominent at 10 dpi) and increased levels of mRNA for Th2 cytokines associated with an anti-inflammatory environment and tissue repair (Annunziato et al., 2015; Gieseck et al., 2018; Kotas and Locksley, 2018), such as IL-5, IL-10, and IL-13 (Figure 4B). Induction of an anti-inflammatory microenvironment was confirmed by RNAscope analysis, which showed that levels of *Ilf10* mRNA expression were higher than those of *Ilfng* mRNA in C57BL/6 mice infected with the genotoxigenic *Salmonella* (Figure 4C). In accordance with the presence of a restorative response, the profile of virtually all macrophages present in the colon of mice infected with the MC1 TT strain exhibited

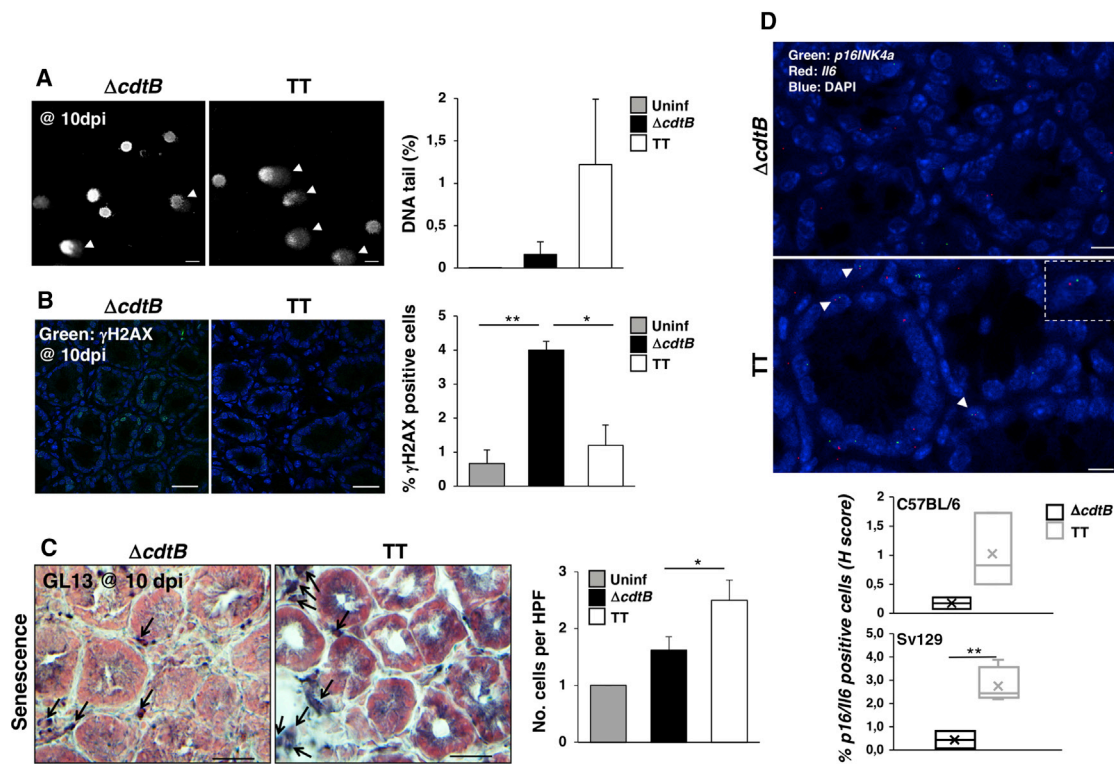


**Figure 2. Senescence induced by infection with the genotoxigenic *Salmonella* is uncoupled from the inflammatory response**

Sv129 mice were mock infected with PBS or infected with the MC1  $\Delta cdtB$  ( $\Delta cdtB$ ) or MC1 TT (TT) strains for 10 days. The data presented are relative to the necropsy performed at 10 dpi.

(A) DNA fragmentation. Left: representative micrograph of SYBR-Gold-stained nuclei. Scale bar, 10  $\mu$ M. Right: quantification comet tail. Data are reported as the mean of the median value of the % DNA in the comet tail for each experimental group. Minimum of 150 cells were evaluated for each mouse (n = 5 mice).

(B) Phosphorylation of histone H2AX ( $\gamma$ H2AX) assessed by immunofluorescence analysis (green). Nuclei were counterstained with DAPI (blue). Left: a representative micrograph of the colonic mucosa. Scale bar, 50  $\mu$ M. Right: quantification of the percentage of  $\gamma$ H2AX-positive cells. At least 500 cells were evaluated for each mouse. \*p  $\leq$  0.05, \*\*p  $\leq$  0.01 (n = 5 mice, mean  $\pm$  SEM).

(C) Senescent cells were detected using the SenTraGor reagent. Left: a representative micrograph of the colonic mucosa. Scale bar, 20  $\mu$ M. Black arrows indicate GL13-positive cells. Right: quantification of the senescent positive cells. \*p  $\leq$  0.05 (n = 5 mice, mean  $\pm$  SEM).

(D) RNAscope analysis to assess the levels of expression of mRNA specific for *p16INK4a* (green) and *Il6* (red) in C57BL/6 mice infected with the MC71  $\Delta cdtB$  ( $\Delta cdtB$ ) or MC71 TT (TT) strains or Sv129 mice infected with the MC1  $\Delta cdtB$  ( $\Delta cdtB$ ) or MC1 TT (TT) strains for 10 days. Top: representative micrograph of the colonic mucosa. White arrowheads indicate cells double positive for *p16INK4a* and *Il6* mRNA. Scale bar, 10  $\mu$ M. The dotted square shows a double-positive cell at a higher magnification. Bottom: quantification of cells double positive for *p16INK4a*- and *Il6*-specific mRNA. \*\*p  $\leq$  0.01 (n = 4 mice).

See also [Figures S4–S6](#).

the phenotype of non-inflammatory cells, resembling the profile observed in the colon of uninfected mice ([Figure 4D](#)).

In spite of detection of increased levels of senescent cells in mice infected with the genotoxigenic strain ([Figure 2C](#)), we did not detect any significant difference in the percentage of cells expressing the proliferative or apoptotic markers Ki67 and cleaved caspase-3, respectively ([Figure S6](#)). It is conceivable that the number of TT-induced senescence cells is not sufficiently high to impact the total levels of proliferating cells. These data would further suggest that the amount of toxin produced during the course of infection is quite low, which is consistent with the low levels of  $\gamma$ H2AX-positive cells ([Figures 2B](#) and [S5A](#)), and raises the important question about the physiological levels of bacterial genotoxins produced during the course of a natural infection.

The immune profile data were reproduced in C57BL/6 mice infected with the MC71 TT strain. We observed a similar extent of

NF- $\kappa$ B activation as well as an enrichment in CD206-positive macrophages and FOXP3-positive regulatory T lymphocytes ( $T_{reg}$ ) ([Whibley et al., 2019](#)) compared to the levels observed in mice infected with the control strain ([Figure S5A](#)).

Having established a link between the presence of a functional genotoxin and modulation of the host response, we assessed whether this effect is regulated by the ATM kinase ([Shiloh and Ziv, 2013](#)). To this end, C57BL/6 ATM wild-type (WT) mice or heterozygotes for the *ATM* gene (denoted as ATM) were infected with the MC71 TT strain for 10 days. We performed immunohistochemical analysis with specific markers for activation of DDR ( $\gamma$ H2AX), senescence (GL13), NF- $\kappa$ B (p65), non-inflammatory macrophages (CD206), and  $T_{reg}$  (FOXP3).

No significant macroscopic difference in the histological score of the small intestine was detected ([Figure S7](#)). As shown in [Figure 5A](#), we observed a decrease in senescence and translocation of the NF- $\kappa$ B subunit p65, and both processes were

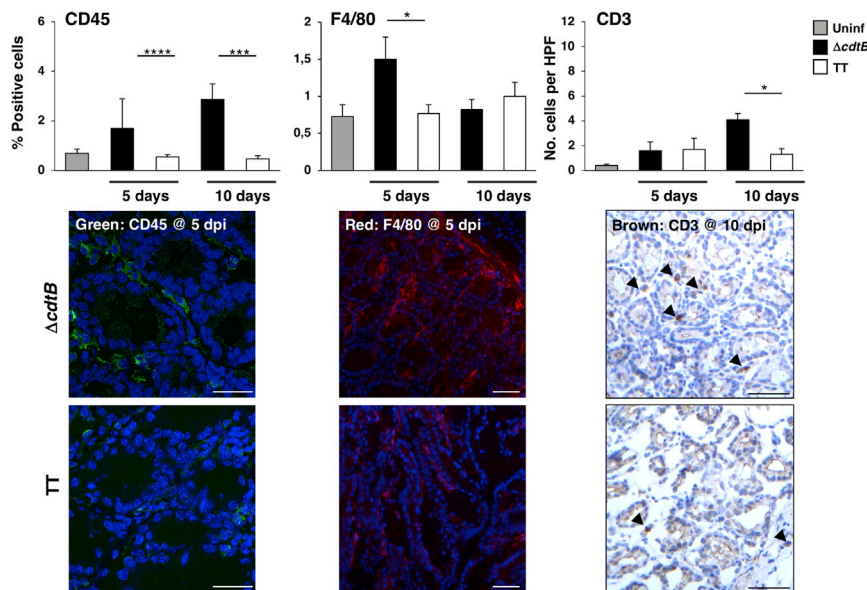


**Figure 3. Lack of inflammatory response induced by the genotoxigenic *Salmonella* is associated with reduced levels of immune cells in the intestinal mucosa**

Sv129 mice were mock infected with PBS (Uninf) or infected with the MC1  $\Delta cdtB$  ( $\Delta cdtB$ ) or MC1 TT (TT) strains for 5 and 10 days. The presence of immune cells was detected by immunofluorescence or histochemistry using the rabbit anti-CD45 specific antibody as a leukocyte marker (left panel, green; scale bar, 50  $\mu$ M), the mouse anti-F4/80 specific antibody as macrophage marker (center panel, red; scale bar, 100  $\mu$ M), or a mouse anti-CD3 specific antibody as a pan T lymphocyte marker (right panel, brown; scale bar, 100  $\mu$ M). Top: quantification of positive cells (mean  $\pm$  SEM). \* $p \leq 0.05$ ; \*\*\* $p \leq 0.001$ ; \*\*\*\* $p \leq 0.0001$  ( $n = 5$  mice). Bottom: representative micrographs taken at 5 dpi for CD45 and F8/40 and 10 dpi for CD3.

shown to be ATM dependent (Kang et al., 2017; Mallette et al., 2007; Miyamoto, 2011). Furthermore, we observed an increase in the percentage of cells positive for  $\gamma$ H2AX, which can be mediated by the related DNA-dependent protein kinase (DNA-PK) (Stiff et al., 2004), suggesting a sustained DDR due to an inefficient DNA repair (Blackford and Jackson, 2017). Using an independent assessment of senescence based on the co-expression of *p16INK4a*- and *Il6*-specific mRNA, we confirmed the trend for a decrease in the levels of senescent cells in the ATM-deficient mice (Figure 5B). This effect was associated with a reduction in the number of  $T_{reg}$  (Figure 5A), but no significant differences in the percentage of M2-like macrophages were observed.

Collectively, these data indicate that the TT immunomodulatory effects are partially dependent on the ATM kinase.

### The anti-inflammatory effect of the TT is lost in subjects affected by colitis

To assess whether the anti-inflammatory effect of the genotoxigenic *Salmonella* strain was maintained in subjects with acute colitis, we infected Sv129 mice with the MC1 TT or control MC1  $\Delta cdtB$  strains 7 days after one cycle administration of dextran sulfate sodium salt (DSS), as summarized in Figure S8A. Infection with both *Salmonella* strains did not affect the disease activity index or amount of fecal lipocalin-2, an inflammatory marker (Chassaing et al., 2012) (Figure S8B). Histological analysis showed that preexisting colitis completely prevents the TT-induced tissue protective immune response observed in healthy mice, since we did not observe any significant difference in the severity of colitis, leukocyte infiltration, and number of PPs in the infected mice, independently of bacterial strain (Figures 6A–6C). The effect detected at histological levels was paralleled by the failure of the genotoxigenic bacteria to reduce the levels of leukocytes (CD45), macrophages (F4/80), and CD3 T lymphocytes in infected mice. However, we observed a time shift in the recruitment of leukocytes and macrophages, which peaked at 5 dpi in mice infected with the control *Salmonella* MC1

$\Delta cdtB$  strain and at 10 dpi in uninfected and MC1-TT-infected mice (Figure 7A). We did not observe differences in the percentage of cells positive for the senescence marker GL13 upon infection with the two *Salmonella* strains, which was higher compared to the levels of senescent cells detected in uninfected mice. These data suggest that the combined effect of DSS treatment and bacterial infection promotes a senescent phenotype associated with inflammation-induced DNA damage (Wei and Ji, 2018).

Interestingly, colitis significantly enhanced colonization with genotoxin-producing bacteria in the colon, and a similar trend was also observed in the mesenteric lymph nodes, although the difference was not statistically significant in the latter ( $p = 0.063$ ) (Figure 7B).

## DISCUSSION

We have previously shown that infection with *S. Typhimurium* expressing a functional TT suppresses specifically intestinal inflammation in otherwise healthy mice (Del Bel Belluz et al., 2016). We have confirmed now this observation (Figures 1 and S3) and further demonstrated that a genotoxin induces DNA fragmentation in an *in vivo* model (Figures 2 and S4). Interestingly, this effect was not associated with a strong induction of  $\gamma$ H2AX, which was higher in the mucosa of mice infected with the control strain (Figure 2). These data suggest that the type of DNA damage induced in the two conditions is different: (1) oxidative-stress induces DNA DSBs in the context of a strong inflammatory response (Kay et al., 2019), which trigger H2AX phosphorylation; and (2) single-strand breaks (SSBs) are induced by low doses of TT, which can be converted to DSBs during S phase, as previously shown for the *E. coli* CDT (Fedor et al., 2013). It is likely that in non-inflammatory conditions the number of proliferating cells in the intestinal mucosa is low, thus limiting the number of  $\gamma$ H2AX positive cells.

We further show that the presence of a functional toxin maintains the tolerogenic environment of the intestinal mucosa (Liu

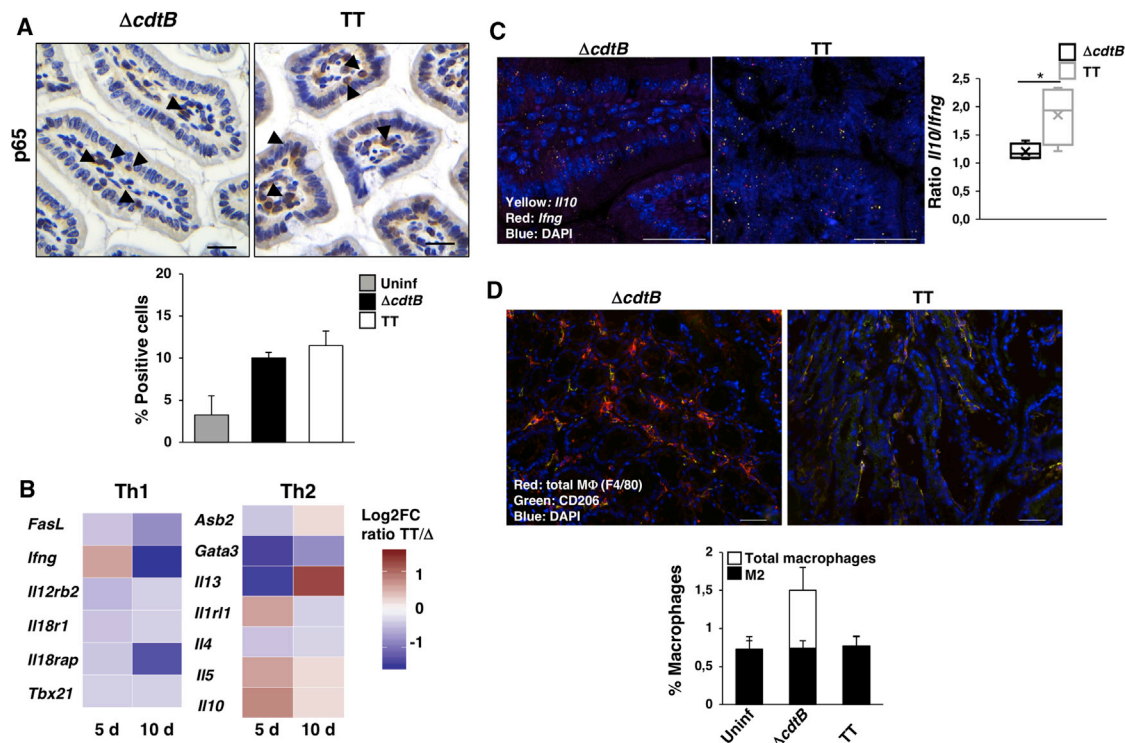


**Figure 4. Infection with the genotoxigenic *Salmonella* induces a type 2 immune response**

Sv129 mice were mock infected with PBS (Uninf) or infected with the MC1 *ΔcdtB* (*ΔcdtB*) or MC1 TT (TT) strains.

(A) Immunohistochemical analysis performed with an anti-p65-specific antibody to detect nuclear translocation of NF- $\kappa$ B at 10 dpi. Top: representative micrograph. Scale bar, 50  $\mu$ M. Bottom: quantification of cells with p65 nuclear localization (n = 5 mice, mean  $\pm$  SEM).

(B) qPCR-array analysis of 84 genes involved in T cell differentiation/polarization in colon of mice at 5 and 10 dpi. Log<sub>2</sub> fold changes of mice infected with the MC1 TT strain versus the MC1 *ΔcdtB* strain (n = 5 mice) are displayed for Th1 and Th2 genes, respectively.

(C) RNAscope analysis to assess the levels of expression of mRNA specific for *Il10* (yellow) and *Ifng* (red) in C57BL/6 mice infected with the MC71 *ΔcdtB* (*ΔcdtB*) or MC71 TT (TT) strains. Left: representative confocal micrograph. Scale bar, 100  $\mu$ M. Right: quantification of the level of mRNA expression. The data are presented as ratio between levels of *Il10* mRNA and *Ifng* mRNA. \*p  $\leq$  0.05 (n = 4 mice).

(D) Analysis of the macrophage population was performed with the pan-macrophage F4/80-specific antibody, followed by a TRITC-conjugated secondary antibody (red), and the CD206 antibody for non-inflammatory macrophages, followed by fluorescein isothiocyanate (FITC)-conjugated secondary antibody (green). Nuclei were counterstained with DAPI (blue) in the intestinal mucosa at 5 dpi. Top: representative micrograph. Scale bar, 100  $\mu$ M. Bottom: quantification of F4/80- and CD206-positive cells (mean  $\pm$  SEM).

See also Figure S5.

et al., 2018; Mowat, 2018) by reducing the recruitment of leukocytes, macrophages, and T lymphocytes, maintaining a robust presence of non-inflammatory macrophages, T<sub>reg</sub>, and increased mRNA levels of Th2 cytokines (Figures 3, 4, and S5), in spite of a significant activation of the transcription factor NF- $\kappa$ B and promotion of cellular senescence (Figure 2 and Figure 4). The anti-inflammatory profile (levels of T<sub>reg</sub> and, to a lesser extent, macrophages) was partially dependent on ATM, the DNA damage transducer (Figure 5), suggesting that the ATM-dependent immunomodulation in response to TT-induced DNA damage is important to promote a delicate equilibrium between Th1- and Th2-like responses to allow a stealth invasion (Dougan and Baker, 2014) and efficient bacterial spread from host to host while reducing the immunopathology.

The TT immunoprotective effect was lost when infection occurred in mice with preexisting acute colitis (Figures 6 and 7), indicating the importance of the tissue microenviron-

ment and suggesting that the immunological profile in which infection occurs (e.g., normal versus inflamed tissue) is very important in defining the final outcome of the effects of TT.

These data highlight a complex interplay between the DNA damage response and modulation of the host response upon infection with *Salmonella*, and we propose that the DDR is not only activated in a cell-autonomous manner to eliminate cells with damaged DNA but plays also a non-cell-autonomous role in shaping the host immune response in a tissue-specific manner that is not exclusively associated with activation of a pro-inflammatory response (Härtlova et al., 2015; Li and Chen, 2018; Nakad and Schumacher, 2016).

#### DDR and immunomodulation

The role of the DDR and the kinases ATM and DNA-dependent protein kinase (DNA-PKcs) in immunomodulation is gaining a lot of interest and it has been proposed that DNA breaks

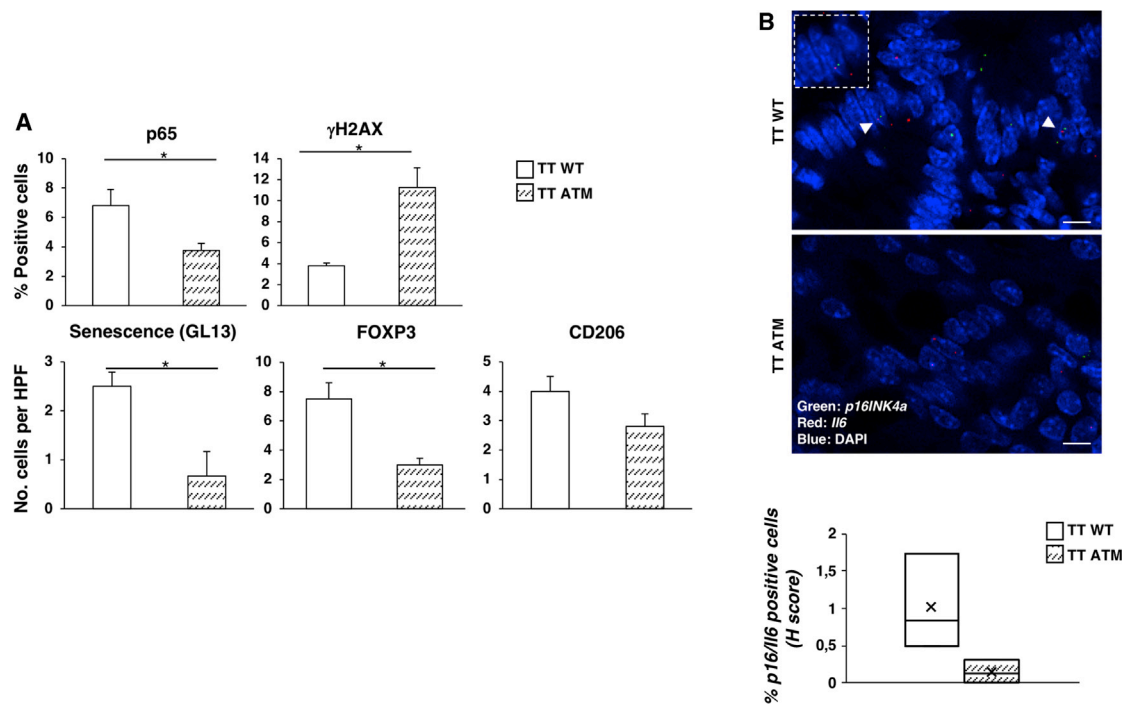


**Figure 5. Absence of a functional ATM alters the response to the genotoxigenic *Salmonella***

C57BL/6 wild-type (WT) mice or ATM heterozygotes (ATM) were infected with the MC71 TT (TT) strain for 10 days.

(A) The following parameters were assessed by immunohistochemistry analysis: phosphorylation of H2AX ( $\gamma$ H2AX), senescence, activation of NF- $\kappa$ B (nuclear translocation of p65), and presence of non-inflammatory macrophages (CD206) and regulatory T cells (FOXP3). \* $p \leq 0.05$  ( $n = 5$  mice, mean  $\pm$  SEM).

(B) RNAscope analysis to assess the levels of expression of mRNA specific for *p16INK4a* (green) and *116* (red). Upper panel: a representative micrograph of the intestinal mucosa. White arrowheads indicate cells double positive for *p16INK4a* and *116* mRNA. Scale bar, 10  $\mu$ M. The dotted square shows a double-positive cell at a higher magnification. Bottom: quantification of the cells double positive for *p16INK4a* and *116* mRNA ( $n = 3$  mice for WT and  $n = 4$  mice for ATM).

and the consequent response activate a cell-specific non-canonical DDR (ncDDR) that regulates the activity of these cells (reviewed in [Bednarski and Sleckman, 2019](#); [Shiloh and Ziv, 2013](#)). Activation of the ATM and DNA-PKcs ncDDR in bone-marrow-derived macrophages is dependent on nitric-oxide-induced DSB in response to *Listeria monocytogenes* infection or stimulation with Toll-like receptor agonists (e.g. Lipopolysaccharide [LPS]). This response triggers a genetic program characterized by upregulation of a broad panel of chemokines, cytokines, and inflammasome activation, with consequent production of IL-1 $\beta$  and IL-18 ([Morales et al., 2017](#)). The relevance of ATM-dependent inflammasome activation to promote efficient bacterial clearance was shown by the enhanced susceptibility to pulmonary infection by *Streptococcus pneumoniae* in ATM-deficient mice ([Erttmann et al., 2016](#)). Interestingly, activation of the ncDDR in macrophages requires signaling from type I IFN receptors, indicating that the pathway activated by type I IFN precedes ([Morales et al., 2017](#)) and is not a consequence of the formation of DNA breaks.

The activation of an immunoregulatory ncDDR may explain why bacteria have acquired, maintained, and horizontally transferred bacterial effectors that can promote DNA damage, which does not kill immediately most of its target cells *in vitro* (reviewed in [Martin and Frisan, 2020](#)) and does not promote apoptosis

above the levels observed in the mucosa of uninfected mice ([Figure S6](#)).

Our results support a scenario where activation of the ATM-dependent DDR promotes activation of an anti-inflammatory immune response more prone to tissue protection and repair ([Annunziato et al., 2015](#); [Gieseck et al., 2018](#); [Kotas and Locksley, 2018](#)). This scenario is supported by the observation that ATM deficiency increases the mortality rate upon DSS-induced colitis ([Westbrook and Schiestl, 2010](#)). This effect is associated with upregulation of mRNA for pro-inflammatory cytokines (e.g., TNF $\alpha$ , IL-12 $\beta$ , IL-23, and IL-6) and a higher percentage of activated CD44-positive T cells, a marker strongly associated with the Th17 population. In line with this observation, inhibition of ATM skews the polarization of T lymphocytes derived from rheumatoid arthritis patients toward Th1 and Th17, imposing a hyperinflammatory phenotype ([Yang et al., 2016](#)). In addition, DNA damage induced by low doses of epirubicin induces an ATM-autophagy-dependent protective effect in the lung tissue of septic mice, resulting in enhanced survival ([Figueiredo et al., 2013](#)).

Based on these observations, it is conceivable that the DDR can exert multiple functions leading to different outcomes, depending on the context: (1) activation of an inflammatory response triggered by the cGAS-STING or via activation of IFN and NF- $\kappa$ B signaling pathways by components of

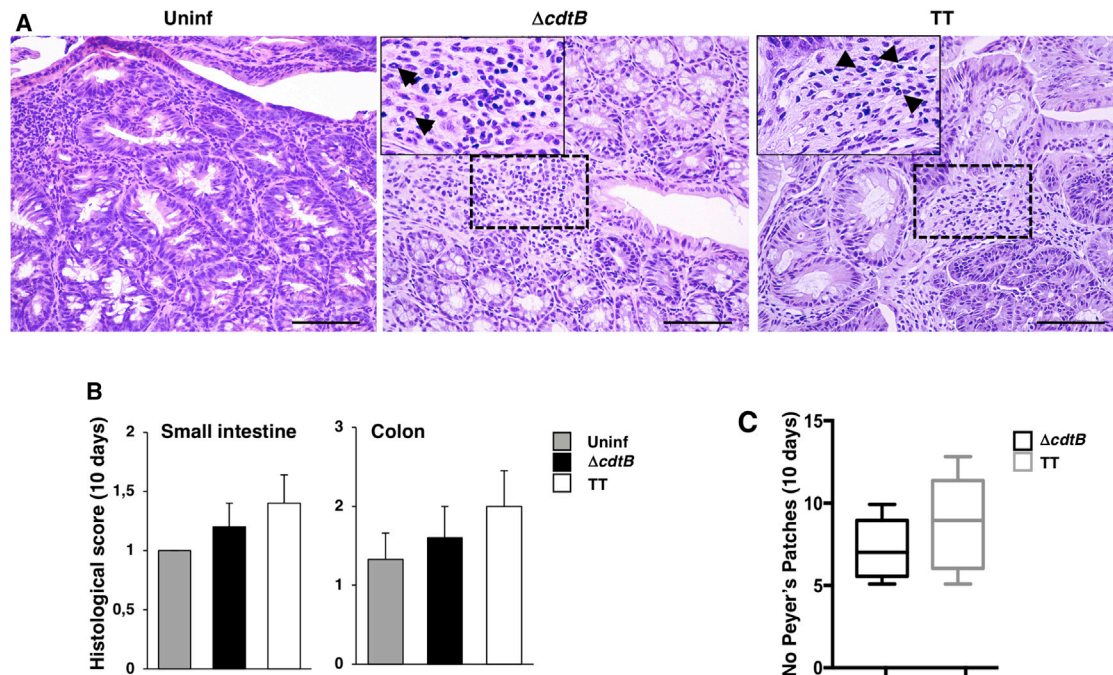


**Figure 6. Preexisting colitis abolishes the anti-inflammatory effect of genotoxic *Salmonella***

Sv129 mice were treated with 2.5% DSS in drinking water for 7 days and then mock infected with PBS (Uninf) or infected with the MC1  $\Delta cdtB$  ( $\Delta cdtB$ ) or MC1 TT (TT) strains for 10 days.

(A) Representative micrograph of the hematoxylin and eosin staining of colon (necropsy performed at 10 dpi). Black arrowheads within the inserts depict examples of infiltrating neutrophils. Scale bar, 100  $\mu$ m.

(B) Histological scores of small intestine and colon. No statistical difference was observed among the samples ( $n = 5$  mice, mean  $\pm$  SEM).

(C) Quantification of the macroscopically visible PPs. No statistical difference was observed among samples ( $n = 5$  mice).

See also Figure S8.

the DNA damage sensors such as the DNA-PK, ATM, and Mre11 (Härtlova et al., 2015; Li and Chen, 2018; Nakad and Schumacher, 2016) to eliminate dangerous cells; (2) activation of cell-specific genetic programs aimed at an efficient activation of anti-microbial immunity (Ertmann et al., 2016; Morales et al., 2017); and (3) fine tuning of the inflammatory response to avoid extensive inflammation-induced tissue damage (Figueiredo et al., 2013; Westbrook and Schiestl, 2010; Yang et al., 2016). Consequently, bacteria may have hijacked this immunomodulatory function, and microbial-induced DNA damage promotes stealth invasion and persistent infections (Del Bel Belluz et al., 2016). The effect observed for TT may also be applied to other members of this family, where toxin-induced DNA damage modulates the host immune response to promote a suitable niche for the microbe, and the end result of this immunomodulatory activity can vary depending on the bacterium lifestyle and tissue tropism.

The open question is how the ATM-induced DDR can promote different outcomes ranging from pro-inflammatory to tissue protective. It is conceivable that both the extent of the DNA damage and the immunological profile of the tissue affected by the insult exert a relevant role in determining the host response (see also the section on senescence and inflammation).

### Senescence and inflammation

Cellular exposure to genotoxins *in vitro* has been shown to induce cellular senescence (Blazkova et al., 2010; Ibler et al., 2019; Secher et al., 2013). SASP is mainly regulated by the pro-inflammatory transcription factor NF- $\kappa$ B (Ohanna et al., 2011), triggered by ATM activation of the DDR, as well as by C/ERBP $\beta$  and MAPKp38 (reviewed in Ohanna et al., 2011). The secretome of senescent cells can promote an alteration of the local microenvironment, including maintaining tissue homeostasis (e.g., tissue remodeling or repair), generating a tumorigenic barrier to prevent cellular transformation, or exerting tumor promoting effects in a context-dependent manner (reviewed in Faget et al., 2019; Rodier and Campisi, 2011).

Interestingly, the composition of SASP is very complex and can differ depending on the cellular origin as well as the senescence-inducing stimulus; however, the pro-inflammatory cytokines IL-1 and IL-6 are reported as commonly secreted mediators in DNA-damage-induced senescence (reviewed in Gorgoulis et al., 2019). In line with these observations, genotoxin-induced senescent cells *in vitro* secrete a plethora of mediators that support their pro-inflammatory role (Blazkova et al., 2010; Secher et al., 2013). Our data demonstrate that infection with a genotoxin-producing bacterium induces senescence *in vivo* and that the presence of senescent cells is associated with an anti-inflammatory response, and to the best of our knowledge, this was not shown previously

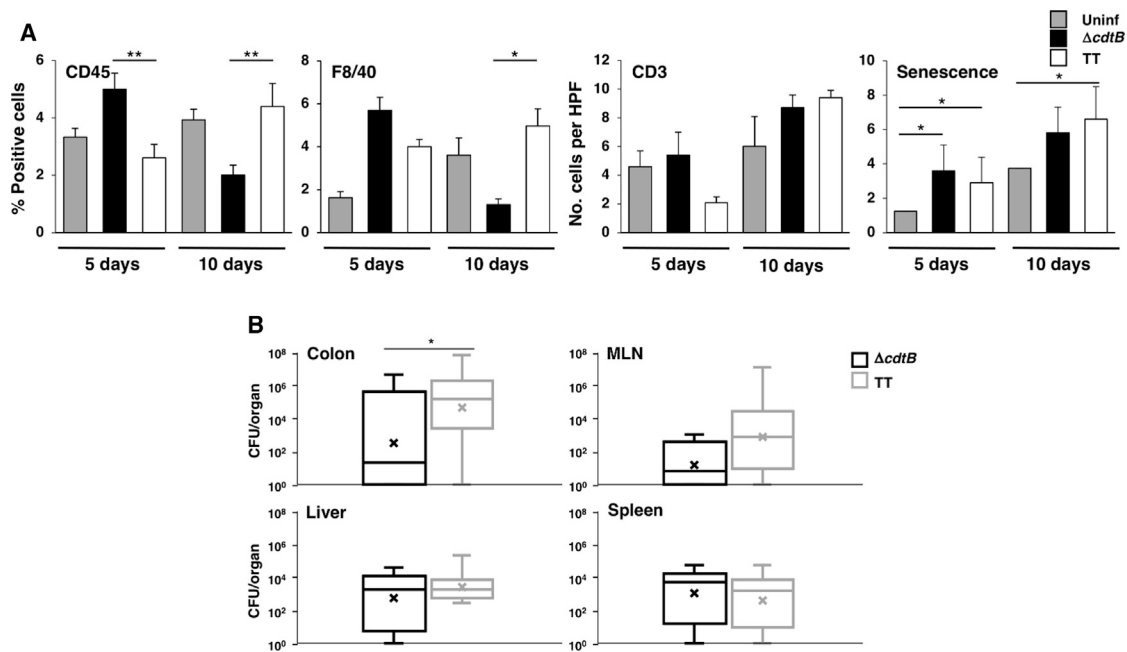


**Figure 7. Preexisting colitis does not prevent infiltration of immune cells but favors colonization with genotoxic *Salmonella***  
Sv129 mice were treated with 2.5% DSS in drinking water for 7 days and then mock infected with PBS (Uninf) or infected with the MC1  $\Delta cdtB$  ( $\Delta cdtB$ ) or MC1 TT (TT) strains for 5 and 10 days.  
(A) The presence of leukocytes (CD45), macrophages (F4/80), T lymphocytes (CD3), and senescent cells was assessed as described in Figures 2 and 3. \* $p \leq 0.05$ , \*\* $p \leq 0.01$  ( $n = 5$  mice, mean  $\pm$  SEM).  
(B) Bacteria dissemination in colon, mesenteric lymph nodes (MLNs), liver, and spleen was assessed at 10 dpi. Data are presented as colony-forming units (CFUs) per organ. \* $p \leq 0.05$  ( $n = 8$  mice from two independent infection experiments).

in any *in vivo* model (Figures 1, 2, 3, 4, S2, and S3). It is noteworthy that the anti-inflammatory effect of the MC1 TT strain was observed only in the intestine and only when infection occurs in healthy mice and not in subjects with preexisting colitis ((Del Bel Belluz et al., 2016) and Figures 1 and 6 and 7). These data suggest that the type of cells (intestinal epithelial cells) and/or the type of tolerogenic environment, characterized by  $T_{reg}$  and non-inflammatory macrophages, may promote the induction of different subsets of senescent cells that contribute to the anti-inflammatory effect, hypothesizing a link between senescence and anti-inflammatory response. The higher presence of p16INK4a-positive cells co-expressing mRNA for the anti-inflammatory cytokine IL-10 in mice infected with the genotoxic strain supports this possibility (Figure S5).

A possible candidate to promote an anti-inflammatory SASP is the Janus kinases (JAK)2-activated Signal transducer and activator of transcription (STAT)3 transcription factor, which has been shown to promote an immune-suppressive SASP profile in PTEN-deficient prostate cancer, characterized by secretion of IL-10 and IL-13 (Toso et al., 2014), two of the Th2 cytokines whose mRNA levels were upregulated in mice infected with the MC1 TT strain (Figure 4). Considering the tissue-specific and context-specific response (intestine versus liver and healthy versus colitis), it is possible that the fine-tuning of the DDR response and consequent SASP phenotype is modulated by the immunological profile of a specific microenvironment, a tissue-based education of senescence, which parallels the

concept of tissue class control of the immune response (Matzinger and Kamala, 2011).

The development of complex organotypic models is required to verify whether (1) different subsets of senescent cells contribute to define the types of host immune response and (2) the immunological profile of the microenvironment imposes a specific type of senescence phenotype.

### Concluding remarks

We have highlighted a complex crosstalk between the DDR induced by TT and the regulation of the host immune response in bacterial infection, which is not only associated with sensing dangerous signals and activating the innate immunity but also shapes the type of immune response shifting from a pro-inflammatory response normally induced by *S. Typhimurium* toward the activation of tissue protective response. The outcome resembles infection with *S. Typhi*, characterized by lack of intestinal inflammation and a stealth invasion of the mucosa (Hiyoshi et al., 2018). However, our data highlight that the anti-inflammatory effect is context-dependent, since it is lost in subjects with preexisting inflammatory conditions. In addition, the presence of senescent cells in the absence of a strong inflammatory response in healthy subjects suggests that the overall effect of the senescence secretory phenotype depends on the tissue-specific microenvironment.

Several questions still need to be addressed, including the role of the immunological profile in the definition of the SASP, the impact of chromatin alterations (including  $\gamma$ H2AX dynamics on

SASP heterogeneity), the characterization of tissue- and context-dependent types of senescence, and the long-term consequences of infection with the genotoxigenic *Salmonella* in subjects with preexisting colitis (Figure 7).

## STAR★METHODS

Detailed methods are provided in the online version of this paper and include the following:

- KEY RESOURCES TABLE
- RESOURCE AVAILABILITY
  - Lead contact
  - Materials availability
  - Data and code availability
- EXPERIMENTAL MODEL AND SUBJECT DETAILS
  - Ethical consideration
  - Mouse strains
  - Bacterial strains
- METHOD DETAILS
  - DSS treatment
  - Infection
  - Histological analysis
  - Senescence staining
  - Comet assay
  - Immunofluorescence and immunohistochemistry
  - Immunofluorescence (fresh frozen tissue)
  - Immunohistochemistry (formalin fixed paraffin embedded tissues, FFPE)
  - Antibodies
  - RT2 profiler PCR array
  - RNAscope
- QUANTIFICATION AND STATISTICAL ANALYSIS

## SUPPLEMENTAL INFORMATION

Supplemental information can be found online at <https://doi.org/10.1016/j.celrep.2021.108931>.

## ACKNOWLEDGMENTS

We are grateful to Drs. Lisa Del Bell Belluz and Boris Mihaljevic for technical assistance with the infection of ATM mice and the RT<sup>2</sup> profiler PCR array, respectively. We acknowledge the Biochemical Imaging Center Umeå (BICU) at Umeå University and the National Microscopy Infrastructure (NMI) (VR-RFI 2016-00968) for providing assistance with microscopy. This investigation was supported by grants from the Swedish Cancer Society (CAN 2017/315 and 20 0699 PjF), the Swedish Research Council (2018-02521), the Kempeförelserna (JCK-1826), the Cancer Research Foundation in Northern Sweden (AMP20-993 and AMP 17-884), and Umeå University (to T.F.) and the German Academic Scholarship Foundation and Erasmus+ (to D.B.).

## AUTHOR CONTRIBUTIONS

O.C.B.M., I.S.P., and T.F. designed the research; O.C.B.M., E.P., A.B., M.L.C., D.B., S.D.P.T., M.M.H., E.B.-R., A.W., I.S.P., and T.F. performed the experiments; O.C.B.M., A.B., M.L.C., D.B., M.M.H., T.T., V.G., T.F., and I.S.P. analyzed data; T.M. and M.R. provided mouse and bacterial strains; and T.F. wrote the manuscript with the help of O.C.B.M. and I.S.P. All authors commented on the manuscript

## DECLARATION OF INTERESTS

The authors declare no competing interests.

Received: January 27, 2020

Revised: October 28, 2020

Accepted: March 11, 2021

Published: April 6, 2021

## REFERENCES

- Annunziato, F., Romagnani, C., and Romagnani, S. (2015). The 3 major types of innate and adaptive cell-mediated effector immunity. *J. Allergy Clin. Immunol.* *135*, 626–635.
- Bednarski, J.J., and Sleckman, B.P. (2019). At the intersection of DNA damage and immune responses. *Nat. Rev. Immunol.* *19*, 231–242.
- Blackford, A.N., and Jackson, S.P. (2017). ATM, ATR, and DNA-PK: The Trinity at the Heart of the DNA Damage Response. *Mol. Cell* *66*, 801–817.
- Blazkova, H., Krejčíková, K., Moudry, P., Frisan, T., Hodny, Z., and Bartek, J. (2010). Bacterial intoxication evokes cellular senescence with persistent DNA damage and cytokine signalling. *J. Cell. Mol. Med.* *14*, 357–367.
- Campisi, J., and d'Adda di Fagagna, F. (2007). Cellular senescence: when bad things happen to good cells. *Nat. Rev. Mol. Cell Biol.* *8*, 729–740.
- Carter, P.B., and Collins, F.M. (1974). Growth of typhoid and paratyphoid bacilli in intravenously infected mice. *Infect. Immun.* *10*, 816–822.
- Chassaing, B., Srinivasan, G., Delgado, M.A., Young, A.N., Gewirtz, A.T., and Vijay-Kumar, M. (2012). Fecal lipocalin 2, a sensitive and broadly dynamic non-invasive biomarker for intestinal inflammation. *PLoS ONE* *7*, e44328.
- Clements, M.O., Eriksson, S., Thompson, A., Lucchini, S., Hinton, J.C., Normark, S., and Rhen, M. (2002). Polynucleotide phosphorylase is a global regulator of virulence and persistency in *Salmonella enterica*. *Proc. Natl. Acad. Sci. USA* *99*, 8784–8789.
- Del Bel Belluz, L., Guidi, R., Pateras, I.S., Levi, L., Mihaljevic, B., Rouf, S.F., Wrangle, M., Candela, M., Turroni, S., Nastasi, C., et al. (2016). The Typhoid Toxin Promotes Host Survival and the Establishment of a Persistent Asymptomatic Infection. *PLoS Pathog.* *12*, e1005528.
- Dougan, G., and Baker, S. (2014). *Salmonella enterica* serovar Typhi and the pathogenesis of typhoid fever. *Annu. Rev. Microbiol.* *68*, 317–336.
- Erben, U., Loddenkemper, C., Doerfel, K., Spieckermann, S., Haller, D., Heimesaat, M.M., Zeitz, M., Siegmund, B., and Kühl, A.A. (2014). A guide to histomorphological evaluation of intestinal inflammation in mouse models. *Int. J. Clin. Exp. Pathol.* *7*, 4557–4576.
- Erttmann, S.F., Härtlova, A., Sloniecka, M., Raffi, F.A., Hosseinzadeh, A., Edgren, T., Rofougaran, R., Resch, U., Fällman, M., Ek, T., and Gekara, N.O. (2016). Loss of the DNA Damage Repair Kinase ATM Impairs Inflammation-Dependent Anti-Bacterial Innate Immunity. *Immunity* *45*, 106–118.
- Evangelou, K., Lougiakis, N., Rizou, S.V., Kotsinas, A., Kletsas, D., Muñoz-Espín, D., Kastrinakis, N.G., Pouli, N., Marakos, P., Townsend, P., et al. (2017). Robust, universal biomarker assay to detect senescent cells in biological specimens. *Aging Cell* *16*, 192–197.
- Faget, D.V., Ren, Q., and Stewart, S.A. (2019). Unmasking senescence: context-dependent effects of SASP in cancer. *Nat. Rev. Cancer* *19*, 439–453.
- Fedor, Y., Vignard, J., Nicolau-Travers, M.L., Boutet-Robinet, E., Watrin, C., Salles, B., and Mirey, G. (2013). From single-strand breaks to double-strand breaks during S-phase: a new mode of action of the *Escherichia coli* Cytolethal Distending Toxin. *Cell. Microbiol.* *15*, 1–15.
- Figueiredo, N., Chora, A., Raquel, H., Pejanovic, N., Pereira, P., Hartleben, B., Neves-Costa, A., Moita, C., Pedroso, D., Pinto, A., et al. (2013). Anthracyclines induce DNA damage response-mediated protection against severe sepsis. *Immunity* *39*, 874–884.
- Gieseck, R.L., 3rd, Wilson, M.S., and Wynn, T.A. (2018). Type 2 immunity in tissue repair and fibrosis. *Nat. Rev. Immunol.* *18*, 62–76.

- Gorgoulis, V., Adams, P.D., Alimonti, A., Bennett, D.C., Bischof, O., Bishop, C., Campisi, J., Collado, M., Evangelou, K., Ferbeyre, G., et al. (2019). Cellular Senescence: Defining a Path Forward. *Cell* **179**, 813–827.
- Grasso, F., and Frisan, T. (2015). Bacterial Genotoxins: Merging the DNA Damage Response into Infection Biology. *Biomolecules* **5**, 1762–1782.
- Guidi, R., Guerra, L., Levi, L., Stenerlöv, B., Fox, J.G., Josenhans, C., Masucci, M.G., and Frisan, T. (2013a). Chronic exposure to the cytolethal distending toxins of Gram-negative bacteria promotes genomic instability and altered DNA damage response. *Cell. Microbiol.* **15**, 98–113.
- Guidi, R., Levi, L., Rouf, S.F., Puiac, S., Rhen, M., and Frisan, T. (2013b). Salmonella enterica delivers its genotoxin through outer membrane vesicles secreted from infected cells. *Cell. Microbiol.* **15**, 2034–2050.
- Haghjoo, E., and Galán, J.E. (2004). Salmonella typhi encodes a functional cytolethal distending toxin that is delivered into host cells by a bacterial-internalization pathway. *Proc. Natl. Acad. Sci. USA* **101**, 4614–4619.
- Hanahan, D., and Weinberg, R.A. (2011). Hallmarks of cancer: the next generation. *Cell* **144**, 646–674.
- Härtlova, A., Ertmann, S.F., Raffi, F.A., Schmalz, A.M., Resch, U., Anugula, S., Lienenklaus, S., Nilsson, L.M., Kröger, A., Nilsson, J.A., et al. (2015). DNA damage primes the type I interferon system via the cytosolic DNA sensor STING to promote anti-microbial innate immunity. *Immunity* **42**, 332–343.
- Hayden, M.S., West, A.P., and Ghosh, S. (2006). NF-kappaB and the immune response. *Oncogene* **25**, 6758–6780.
- Hernandez-Segura, A., Nehme, J., and Demaria, M. (2018). Hallmarks of Cellular Senescence. *Trends Cell Biol.* **28**, 436–453.
- Herzog, K.H., Chong, M.J., Kapsetaki, M., Morgan, J.I., and McKinnon, P.J. (1998). Requirement for Atm in ionizing radiation-induced cell death in the developing central nervous system. *Science* **280**, 1089–1091.
- Hiyoshi, H., Tiffany, C.R., Bronner, D.N., and Bäuml, A.J. (2018). Typhoidal Salmonella serovars: ecological opportunity and the evolution of a new pathovar. *FEMS Microbiol. Rev.* **42**, 527–541.
- Ibler, A.E.M., ElGhazaly, M., Naylor, K.L., Bulgakova, N.A., F El-Khamisy, S., and Humphreys, D. (2019). Typhoid toxin exhausts the RPA response to DNA replication stress driving senescence and Salmonella infection. *Nat. Commun.* **10**, 4040.
- Kang, H.T., Park, J.T., Choi, K., Kim, Y., Choi, H.J.C., Jung, C.W., Lee, Y.S., and Park, S.C. (2017). Chemical screening identifies ATM as a target for alleviating senescence. *Nat. Chem. Biol.* **13**, 616–623.
- Kay, J., Thadhani, E., Samson, L., and Engelward, B. (2019). Inflammation-induced DNA damage, mutations and cancer. *DNA Repair (Amst.)* **83**, 102673.
- Kotas, M.E., and Locksley, R.M. (2018). Why ILCs? *Immunity* **48**, 1081–1090.
- Krtolica, A., Parrinello, S., Lockett, S., Desprez, P.Y., and Campisi, J. (2001). Senescent fibroblasts promote epithelial cell growth and tumorigenesis: a link between cancer and aging. *Proc. Natl. Acad. Sci. USA* **98**, 12072–12077.
- Li, T., and Chen, Z.J. (2018). The cGAS-cGAMP-STING pathway connects DNA damage to inflammation, senescence, and cancer. *J. Exp. Med.* **215**, 1287–1299.
- Liu, Y.H., Ding, Y., Gao, C.C., Li, L.S., Wang, Y.X., and Xu, J.D. (2018). Functional macrophages and gastrointestinal disorders. *World J. Gastroenterol.* **24**, 1181–1195.
- Loomis, W.P., Johnson, M.L., Brasfield, A., Blanc, M.P., Yi, J., Miller, S.I., Cookson, B.T., and Hajjar, A.M. (2014). Temporal and anatomical host resistance to chronic Salmonella infection is quantitatively dictated by Nramp1 and influenced by host genetic background. *PLoS ONE* **9**, e111763.
- Mallette, F.A., Gaumont-Leclerc, M.F., and Ferbeyre, G. (2007). The DNA damage signaling pathway is a critical mediator of oncogene-induced senescence. *Genes Dev.* **21**, 43–48.
- Martin, O.C.B., and Frisan, T. (2020). Bacterial Genotoxin-Induced DNA Damage and Modulation of the Host Immune Microenvironment. *Toxins (Basel)* **12**, 63.
- Matzinger, P., and Kamala, T. (2011). Tissue-based class control: the other side of tolerance. *Nat. Rev. Immunol.* **11**, 221–230.
- Miyamoto, S. (2011). Nuclear initiated NF-κB signaling: NEMO and ATM take center stage. *Cell Res.* **21**, 116–130.
- Morales, A.J., Carrero, J.A., Hung, P.J., Tubbs, A.T., Andrews, J.M., Edelson, B.T., Calderon, B., Innes, C.L., Paules, R.S., Payton, J.E., and Sleckman, B.P. (2017). A type I IFN-dependent DNA damage response regulates the genetic program and inflammasome activation in macrophages. *eLife* **6**, e24655.
- Mowat, A.M. (2018). To respond or not to respond - a personal perspective of intestinal tolerance. *Nat. Rev. Immunol.* **18**, 405–415.
- Nakad, R., and Schumacher, B. (2016). DNA Damage Response and Immune Defense: Links and Mechanisms. *Front. Genet.* **7**, 147.
- Nesic, D., Hsu, Y., and Stebbins, C.E. (2004). Assembly and function of a bacterial genotoxin. *Nature* **429**, 429–433.
- Ohanna, M., Giuliano, S., Bonet, C., Imbert, V., Hofman, V., Zangari, J., Bille, K., Robert, C., Bressac-de Paillerets, B., Hofman, P., et al. (2011). Senescent cells develop a PARP-1 and nuclear factor-kappaB-associated secretome (PNAS). *Genes Dev.* **25**, 1245–1261.
- Perdry, H., Gutzkow, K.B., Chevalier, M., Huc, L., Brunborg, G., and Boutet-Robinet, E. (2018). Validation of Gelbond® high-throughput alkaline and Fpg-modified comet assay using a linear mixed model. *Environ. Mol. Mutagen.* **59**, 595–602.
- Pu, X., Wang, Z., and Klaunig, J.E. (2015). Alkaline Comet Assay for Assessing DNA Damage in Individual Cells. *Curr. Protoc. Toxicol.* **65**, 3.12.11–11.
- Rodier, F., and Campisi, J. (2011). Four faces of cellular senescence. *J. Cell Biol.* **192**, 547–556.
- Rogakou, E.P., Boon, C., Redon, C., and Bonner, W.M. (1999). Megabase chromatin domains involved in DNA double-strand breaks in vivo. *J. Cell Biol.* **146**, 905–916.
- Secher, T., Samba-Louaka, A., Oswald, E., and Nougayrède, J.P. (2013). Escherichia coli producing colibactin triggers premature and transmissible senescence in mammalian cells. *PLoS ONE* **8**, e77157.
- Shiloh, Y., and Ziv, Y. (2013). The ATM protein kinase: regulating the cellular response to genotoxic stress, and more. *Nat. Rev. Mol. Cell Biol.* **14**, 197–210.
- Shrivastava, R., and Shukla, N. (2019). Attributes of alternatively activated (M2) macrophages. *Life Sci.* **224**, 222–231.
- Song, J., Gao, X., and Galán, J.E. (2013). Structure and function of the Salmonella Typhi chimaeric A(2)B(5) typhoid toxin. *Nature* **499**, 350–354.
- Spanò, S., Ugalde, J.E., and Galán, J.E. (2008). Delivery of a Salmonella Typhi exotoxin from a host intracellular compartment. *Cell Host Microbe* **3**, 30–38.
- Stiff, T., O'Driscoll, M., Rief, N., Iwabuchi, K., Löbrich, M., and Jeggo, P.A. (2004). ATM and DNA-PK function redundantly to phosphorylate H2AX after exposure to ionizing radiation. *Cancer Res.* **64**, 2390–2396.
- Toso, A., Revandkar, A., Di Mitri, D., Guccini, I., Proietti, M., Sarti, M., Pinton, S., Zhang, J., Kalathur, M., Civenni, G., et al. (2014). Enhancing chemotherapy efficacy in Pten-deficient prostate tumors by activating the senescence-associated antitumor immunity. *Cell Rep.* **9**, 75–89.
- Wei, W., and Ji, S. (2018). Cellular senescence: Molecular mechanisms and pathogenicity. *J. Cell. Physiol.* **233**, 9121–9135.
- Westbrook, A.M., and Schiestl, R.H. (2010). Atm-deficient mice exhibit increased sensitivity to dextran sulfate sodium-induced colitis characterized by elevated DNA damage and persistent immune activation. *Cancer Res.* **70**, 1875–1884.
- Whibley, N., Tucci, A., and Powrie, F. (2019). Regulatory T cell adaptation in the intestine and skin. *Nat. Immunol.* **20**, 386–396.
- Yang, Z., Shen, Y., Oishi, H., Matteson, E.L., Tian, L., Goronzy, J.J., and Weyand, C.M. (2016). Restoring oxidant signaling suppresses proarthritogenic T cell effector functions in rheumatoid arthritis. *Sci. Transl. Med.* **8**, 331ra38.

## STAR★METHODS

### KEY RESOURCES TABLE

REAGENT OR RESOURCE	SOURCE	IDENTIFIER
<b>Antibodies</b>		
Anti-CD45 IgG (1:100)	Abcam	Cat# ab10558; RRID:AB_442810
Anti-F4/80 IgG (1:100)	Bio-Rad	Cat# MCA497G; RRID:AB_872005
Anti-CD206 (1:400)	R&D system	Cat# AF2535; RRID:AB_2063012
Anti- $\gamma$ H2AX (1:200)	Cell Signaling	Cat# 9718; RRID:AB_2118009
Anti-CD3 (1:150)	Abcam	Cat# ab5690; RRID:AB_305055
Anti-CD206 (1:1000)	Abcam	Cat# ab64693; RRID:AB_1523910
Anti-FOXP3 (1:200)	Novus Biologicals	Cat# NB100-39002; RRID:AB_838249
Anti-p65 (1:100)	Santa Cruz	Cat# sc-8008; RRID:AB_628017
Anti-Ki-67 (1:100)	Abcam	Cat# ab16667; RRID:AB_302459
Anti-Cleaved caspase-3 (1:100)	Cell Signaling	Cat# 9661; RRID:AB_2341188
Anti- $\gamma$ H2AX (1:1000)	Merck Millipore	Cat# 05-636; RRID:AB_309864
<b>Bacterial strains</b>		
MC1 TT	Frisan's laboratory	<a href="#">Del Bel Belluz et al., 2016</a>
MC1 $\Delta$ <i>cdtB</i>	Frisan's laboratory	<a href="#">Del Bel Belluz et al., 2016</a>
MC71 TT	Frisan's laboratory	<a href="#">Del Bel Belluz et al., 2016</a>
MC1 $\Delta$ <i>cdtB</i>	Frisan's laboratory	<a href="#">Del Bel Belluz et al., 2016</a>
<b>Chemicals</b>		
DSS	Sigma-Aldrich Merck	42867
RNAlater	Sigma-Aldrich Merck	R0901
Tissue-Tek OCT	Sakura Finetek	4583
SenTraGor®	Lab Supplies Scientific - P. Galanis & Co	AR8850020
VECTASHIELD®	Vector lab	H-1200-10
(DAB) substrate kit	Vector lab	SK-4100
<b>Critical commercial assays</b>		
Lipocalin ELISA	R&D Systems	DY1857
RNeasy Mini Kit	QIAGEN	74104
RNAscope Multiplex Fluorescent Reagent Kit	Bio-techne	323100
Opal 4-Color Manual IHC Kit 50 slides	PerkinElmer	NEL810001KT
<i>p16INK4a</i> target probe	Bio-techne	411011
<i>Il6</i> target probe	Bio-techne	315891-C2
<i>Il10</i> target probe	Bio-techne	317261-C3
<i>Ifng</i> target probe	Bio-techne	311391-C2
RNAscope 3-plex Positive control probe	Bio-techne	320881
RNAscope 3-plex Negative control probe	Bio-techne	320871
<b>Experimental model organisms/strains</b>		
<i>Sv129</i>	Taconic Biosciences	129SVE-F
C57BL/6	Ma's laboratory	<a href="#">Herzog et al., 1998</a>
chloramphenicol resistance cassette (Cm) forward primer 5'- AAAGGAT CCGTGTA GCTGGAGCTGCTTC-3'	Sigma-Aldrich Merck	N/A

(Continued on next page)

<b>Continued</b>		
REAGENT OR RESOURCE	SOURCE	IDENTIFIER
Cm reverse primer 5'-AAAGGTACCCATATGAATATCCTCCTTAG-3'	Sigma-Aldrich Merck	N/A
TT and the Cm forward primer 5'-GT CCGCACGTTCTTCCGTGGCGTGGATATTAGTCAGGTCTTTAGCGCCAAAGATATTGCCATTCTGTAAC TGATAAAGTAGGTGTGCTTA-3'	Sigma-Aldrich Merck	N/A
TT and the Cm reverse primer 5'-AATGCCGCTTTTAATGAGTCGATGACACGACGCCACGAATTTATTGCATATGAATATCCTCCTTAG-3'	Sigma-Aldrich Merck	N/A
<b>Software</b>		
Fiji ImageJ	<a href="https://imagej.net/Fiji/Downloads">https://imagej.net/Fiji/Downloads</a>	doi:10.1038/nmeth.2019
Prism 7 Graph Pad	<a href="https://www.graphpad.com/">https://www.graphpad.com/</a>	N/A
CometScore 2.0	TriTek CometScore V 2.0 software	N/A
<b>Other</b>		
CryoStar NX70	Thermo Scientific	N/A
Laser Scanning Microscopy LSM-510 META	Zeiss	N/A

## RESOURCE AVAILABILITY

### Lead contact

Further information and requests for resources and reagents should be directed to and will be fulfilled by the Lead Contact Teresa Frisan ([teresa.frisan@umu.se](mailto:teresa.frisan@umu.se))

### Materials availability

No new materials were generated for this study, and all materials are commercially available. The bacterial strains are available upon signed Materials Transfer Agreement.

### Data and code availability

Datasets will be made available upon signed Materials Transfer Agreement.

## EXPERIMENTAL MODEL AND SUBJECT DETAILS

### Ethical consideration

All animals were handled in strict accordance with good animal practice as defined by the relevant national animal welfare bodies, following proceedings described in EU legislation. This study was approved by the Regional Animal Studies Ethical Committees, Northern Norrland and Stockholm Norra, Sweden (reference number A17-17 and N112/16) and from the Animal Care Committee, Toronto, Canada (reference number AUP #4088.0).

### Mouse strains

129S6/SvEvTac (herein named Sv129) mice were obtained from Taconic Biosciences Inc. (Bomholt, Denmark). C57BL/6 ATM deficient mice were previously described ([Herzog et al., 1998](#)). Mice were housed in a pathogen-free facility, and female mice were infected at 8 weeks of age.

### Bacterial strains

The *Salmonella* Typhimurium strains MC1 and MC71 of the line SR-11 carrying the typhoid toxin genes and the isogenic control strains were constructed as previously described ([Del Bel Belluz et al., 2016](#)). Briefly, the genes encoding the typhoid toxin (TT) or the toxin carrying a deletion of the active subunit gene *cdtB* ( $\Delta cdtB$ ) were cloned into the pEGFP-C1 plasmid (Clontech Laboratories,

Mountain View, CA, USA) under the control of their endogenous promoters (Guidi et al., 2013b). The gene encoding the chloramphenicol resistance (Cm) was amplified from the pKD3 plasmid (NCBI Gene Bank AY048742), using the following primers: 5'- AAAGGAT CCGTGTAGGCTGGAGCTGCTTC-3' and 5'-AAAGGTACCCATATGAATATCCTCCTTAG-3', and cloned into the BamHI-KpnI sites of the pEGFP-C1-TT or pEGFP-C1- $\Delta$ cdtB plasmids. The toxin and the chloramphenicol genes were amplified using the primers 5'-GT CCGCACGTTCTCCGTGGCGTGGATATTAGTCAGGTCTTTAGCGCCAAAGATATT GCCATTCTGTAAGTATAAAGTAGGTGTGCT TA-3' and 5'-AATGCCGCTTTTAAT GAGTCGATGGACACGACGCCACGAATTTATTGCATATGAATATCCTCCTTAG-3', and transferred by homologous recombination into the genomic *proV* gene of *S. Typhimurium* strain LB5010 carrying the pKD46 plasmid. The MC1/MC71-TT and MC1/MC71- $\Delta$ cdtB strains were produced by P22int phage transduction, and grown overnight in Luria agar plates enriched with Cm (10  $\mu$ g/ml). The construction of these strains was approved by the Swedish Work Environment Authority.

## METHOD DETAILS

### DSS treatment

For the colitis-mimicking experiment, DSS 2.5% (Sigma-Aldrich Merck) was administered in drinking water *ad libitum* for 7 days prior administration of the bacterial strains or vehicle as described above. The Disease Activity Index (DAI) was determined by scoring changes in weight loss (score: 0, none; 1, 1%–5%; 2, 5%–10%; 3, 10%–20%; and 4, > 20%), stool consistency (score: 0, normal; 2, mildly soft; 4, diarrhea), and bleeding (score: 0, normal; 2, traces of blood in stool and 4, visible rectal bleeding). All parameters were scored daily during all the experiment. Feces were collected and resuspended in PBS containing 0.1% Tween-20 (100 mg/ml) and vortexed for 20 minutes until a homogeneous fecal suspension was obtained. Samples were centrifuged at 12,000 rpm for 10 minutes at 4°C to collect clear supernatants. The fecal lipocalin was assessed by ELISA according to the manufacturer instruction (Duoset murine Lcn-2 ELISA kit, R&D Systems, Minneapolis, MN) and as previously described (Chassaing et al., 2012).

### Infection

Mice were housed in a pathogen-free facility, and female mice were infected at 8 weeks of age. We used the *Salmonella* MC1 strains at the infection dose of  $10^8$  for the 129S6/SvEvTac mice. C57BL/6 wild-type and ATM mice were infected with the attenuated MC71 strains (Clements et al., 2002) at the infection dose of  $10^4$  due to their increased susceptibility to *Salmonella* infection (Loomis et al., 2014). Infection was performed as previously described (Del Bel Belluz et al., 2016).

At 5 or 10 days post infection, intestine, liver, spleen, and mesenteric lymph nodes were collected from each mouse, as described in (Del Bel Belluz et al., 2016). Briefly, the cecum, two centimeters of the proximal region of the jejunum, ileum, and colon, one-third of the spleen, and approximately 10 mm<sup>3</sup> of each liver lobe were stored in RNAlater (Sigma-Aldrich, St. Louis, MO, USA) at –80°C for RNA extraction. The remaining jejunum, ileum, and colon, one-third of the spleen, the central region of the liver including the gallbladder were used for histological and immunohistochemical analysis. The tissue was either fixed in 4% paraformaldehyde and paraffin embedded (FFPE) or frozen on dry ice in a cryomold, embedded in Tissue-Tek OCT (Sakura Finetek, Tokyo, Japan). Lymph nodes, cecum content, and the remaining parts of liver and spleen were homogenized in phosphate-buffered saline (PBS) to assess bacterial recovery on Luria broth (LB) plates supplemented with Cm (50  $\mu$ g/ml).

### Histological analysis

The histopathological evaluation of intestinal inflammation was performed on hematoxylin-eosin stained sections according to previously published criteria (Erben et al., 2014). Collectively for the histopathological assessment we employed a scoring system based on the inflammatory cell infiltrate, epithelial changes, and mucosal architecture (Erben et al., 2014).

### Senescence staining

Examination of senescence was performed by a hybrid histo-/immuno chemical assay utilizing GL13 (commercially available as SenTraGor®) which is a lipophilic, biotin-linked Sudan Black-B (SBB) analog (Evangelou et al., 2017). For GL13 evaluation we counted the number of positive cells per high power field (HPF, magnification 400x).

### Comet assay

Genotoxicity on colon mucosa was evaluated by alkaline comet assay. Colon mucosa cells were collected by scraping and stored in HBSS/EDTA 0.024 M buffer at pH 7.5 before slow freezing at –80°C. The alkaline comet assay, was performed as previously described (Perdry et al., 2018). Briefly, cells were resuspended to a final concentration of 0.7% in low-melting point agarose in PBS. Polyester *Gelbond*® films were used to deposit gels and placed on a metal plate on ice for agarose solidification. Films were then immersed in cold lysis buffer (2.5 M NaCl, 0.1 M Na<sub>2</sub>EDTA, 10 mM Tris, 1% Triton x-100, 10% DMSO) for 18 h followed by transfer into freshly prepared alkaline unwinding solution. Electrophoresis was carried out in cold fresh electrophoresis solution (0.3 M NaOH, 1 mM Na<sub>2</sub>EDTA, pH > 13) for 24 min. After electrophoresis, films were immersed in PBS for neutralization, followed by fixation in 100% EtOH for 1.5h and drying. Films were glued onto a glass slide and rehydrated in TE buffer with DNA stain SYBR® Gold for 20 minutes. Image analysis were performed with CometScore 2.0 free software. For each cell, the extent of DNA damage was calculated as percentage of pixels in the comet tail by dividing the measurement of the intensity of all tail pixels by

the total intensity of all pixels in head and tail of comets, as previously described (Perdry et al., 2018). For each animal, the median of minimum 150 cells was determined.

### Immunofluorescence and immunohistochemistry

Formalin-fixed paraffin-embedded 6  $\mu\text{m}$  tissue sections were deparaffinized in xylene and rehydrated through a graded series of alcohol. The endogenous peroxidase activity was blocked by incubating the sections 30 min with 3%  $\text{H}_2\text{O}_2$  in distilled  $\text{H}_2\text{O}$ .

The OCT-embedded tissues were cut with a CryoStar NX70 Cryostat into 6  $\mu\text{m}$  thick sections at  $-20^\circ\text{C}$ , mounted on SuperfrostTM Plus microscope slides, and stored at  $-80^\circ\text{C}$  until usage.

### Immunofluorescence (fresh frozen tissue)

The intestinal sections, small intestine, and colon were fixed in  $-20^\circ\text{C}$  cold acetone for 10 min. After fixation, the sections were washed two times in Tris-buffered saline (TBS) for 5 min and permeabilized with 0.1% Triton 100X, 2% fetal bovine serum (FBS), 1% bovine serum albumin (BSA) in TBS. Subsequent washing in TBS for 2 min was performed and the tissues were incubated with blocking solution (2% FBS, 1% BSA in TBS) for 30 min, followed by incubation with the primary antibodies. After incubation with the primary antibodies for 1 h, the slides were washed two times for 2 min with TBS and incubated for 1 h with the compatible secondary antibodies, used at a dilution of 1:1000 in blocking solution. Subsequently, the slides were washed again three times with TBS for 5 min and finally mounted. The nuclei were counterstained with VECTASHIELD® containing DAPI (Vector Laboratories). All images were acquired with a Zeiss Laser Scanning Microscopy LSM-510 META Confocal Microscope, equipped with a 40X Plan-Neo/1.3 NA objective. At least 500 cells were evaluated for each mouse.

### Immunohistochemistry (formalin fixed paraffin embedded tissues, FFPE)

Antigen retrieval was performed by heat-mediated antigen retrieval method in 10 mM citric acid (pH 6.0). The primary antibodies were incubated at  $4^\circ\text{C}$  overnight. After incubation with the primary antibodies, the slides were washed 3 times with TBS, and incubated with the appropriate Horseradish Peroxidase (HRP)-conjugated secondary antibody for 1 h at a dilution of 1:200 in TBS, supplemented with 1% BSA. Immunocomplexes were visualized with the 3,3'-diaminobenzidine (DAB) substrate kit (SK-4100, Vector Laboratories Inc., Burlingame, CA, USA), according to the instructions of the manufacturer. Sections were counterstained with hematoxylin solution (Sigma-Aldrich). The evaluation of  $\gamma\text{H2AX}$ , p65, Ki67 and cleaved caspase 3 was performed by assessing the percentage (%) of positive epithelial cells. For the assessment of CD3, FOXP3, and CD206, we counted the number of positive cells in the stroma per high power field (HPF, magnification 400x). Slide examination was performed by three independent observers with minimal inter-observer variability.

### Antibodies

The following primary antibodies were used for immunofluorescence analysis: rabbit anti-CD45 IgG (1:100, Abcam), rat anti-F4/80 IgG (1:100, Bio-Rad), goat anti-CD206 (1:400, R&D system), rabbit anti- $\gamma\text{H2AX}$  (1:200, Cell Signaling Technology).

The following primary antibodies were used for immunohistochemistry: anti-CD3 (Abcam, 1:150), anti-CD206 (Abcam, 1:1000), anti-FOXP3 (Novus Biologicals, 1:1200), anti-p65 (Santa Cruz; 1:100), Ki-67 (Abcam, 1:100), cleaved caspase 3 (Cell Signaling, 1:100), anti- $\gamma\text{H2AX}$  (Ser139, Millipore; 1:1000). Antibodies were also sourced using BenchSci (<https://www.benchsci.com>).

### RT2 profiler PCR array

Total RNA from individual mice was isolated using RNeasy Mini Kit (QIAGEN), pooled in equimolar amounts for each experimental group, retrotranscribed using RT<sup>2</sup> First Strand Kit (QIAGEN) according to the manufacturer's instructions and loaded onto qPCR plates (Mouse Cancer Inflammation & Immunity Crosstalk and T cell subsets PCR Array, QIAGEN), and as previously described (Del Bel Belluz et al., 2016). Briefly, cycling was performed as follows:  $95^\circ\text{C}$  for 10 minutes;  $95^\circ\text{C}$  for 15 s and  $60^\circ\text{C}$  for 1 minute for 40 cycles. Raw Ct values were normalized to the geometric mean of five housekeeping genes (Actb, B2m, Gapdh, Gusb, Hsp90ab1). Fold changes in gene expression were calculated with the delta Ct method ( $\Delta\Delta\text{Ct}$ ).

The raw data are reported in Data S1.

### RNAscope

*In situ* detection of mRNA levels for *p16INK4a*, *Il6*, *Il10* and *Irfng* using the RNAscope Multiplex Fluorescent Reagent Kit (Bio-technie, Oxford, UK) was performed according to manufacturer's protocol.

Housekeeping genes *Polymerase II Subunit A (Pol2a)*, *Peptidylpropyl isomerase B (PPIB)* and *Ubiquitin C (UBC)* were used as internal controls to assess the mRNA quality, while the probe targeting the *DapB* mRNA from the *Bacillus subtilis* strain SMY was used as negative control (Figure S5B).

The sections were pretreated either using Protease IV for 15 minutes at room temperature or Protease Plus for 30 minutes at room temperature and further incubated with the probes targeting *p16INK4a*, *Il6*, *Il10* and *Irfng* diluted according to manufacturer protocol for 2 h at  $40^\circ\text{C}$ .

For detection of the targeting probes, the sections were incubated with fluorescent dyes Opal 520, Opal 570 and Opal 690 (1:1000, #NEL810001KT, PerkinElmer). The slides were washed using the supplied washing buffer (Bio-technie, Oxford, UK) after each hybrid-

ization step at room temperature. Nuclei were counterstained with DAPI. Images were acquired with a confocal scanning microscope (Leica TCS SP8, Leica Microsystems, Wetzlar, Germany). Expression levels were assessed quantitatively using H-score, following manufacturer's guidelines.

#### QUANTIFICATION AND STATISTICAL ANALYSIS

All the statistical analyses have been performed using Prism 7 Graph Pad Software. The significance of differences between two experimental groups (mice infected with the control and the genotoxin *Salmonella* strain) was determined by the Student t test. The significance of differences between three experimental groups was determined by ANOVA with Fisher's LSD post-test, while significance of differences between two experimental groups was determined with the Student t test. p values < 0.05 were considered significant.